

# 1 Climatic Controls on Metabolic Constraints in the Ocean

2 Precious Mongwe<sup>1</sup>, Matthew Long<sup>2</sup>, Takamitsu Ito<sup>3</sup>, Curtis Deutsch<sup>4</sup>, and Yeray  
3 Santana-Falcón<sup>5</sup>

4 <sup>1</sup>Southern Ocean Carbon Climate Observatory (SOCCO), CSIR, Cape Town, South Africa

5 <sup>2</sup>Oceanography Section, Climate and Global Dynamics Laboratory, National Center for Atmospheric Research,  
6 Boulder, CO, United States of America

7 <sup>3</sup>School of Earth and Atmospheric Sciences, Georgia Institute of Technology, Atlanta, Georgia United States of  
8 America

9 <sup>4</sup>Department of Geosciences, Princeton University, Princeton, NJ, United States of America

10 <sup>5</sup>CNRM, Université de Toulouse, Météo-France, CNRS, Toulouse, 31057, France

11 **Corresponding Author:** Precious Mongwe (pmongwe@csir.co.za)

## 13 Abstract

14 Observations and models indicate that climate warming is associated with the loss of dissolved  
15 oxygen from the ocean. Dissolved oxygen is a fundamental requirement for heterotrophic marine  
16 organisms (except marine mammals) and, since the basal metabolism of ectotherms increases  
17 with temperature, warming increases organisms' oxygen demand. Therefore, warming and  
18 deoxygenation pose a compound threat to marine ecosystems. In this study, we leverage an  
19 ecophysiological framework and compilation of empirical trait data quantifying the temperature  
20 sensitivity and oxygen requirements of metabolic rates for a range of marine species  
21 ("ecotypes"). Using the Community Earth System Model Large Ensemble, we investigate how  
22 natural climate variability and anthropogenic forcing impact the ability of marine environments  
23 to support aerobic metabolisms on interannual to multi-decadal timescales. Warming and  
24 deoxygenation projected over the next several decades will yield a reduction in the volume of  
25 viable ocean habitat. We find that fluctuations in temperature and oxygen associated with natural  
26 variability are distinct from those associated with anthropogenic forcing in the upper ocean.  
27 Further, the joint temperature-oxygen anthropogenic signal emerges sooner than independently  
28 from natural variability. Our results demonstrate that anthropogenic perturbations underway in  
29 the ocean will strongly exceed those associated with the natural system; in many regions,  
30 organisms will be pushed closer to or beyond their physiological limits, leaving the ecosystem  
31 more vulnerable to extreme temperature-oxygen events.

## 32 **1. Introduction**

33 Dissolved oxygen (O<sub>2</sub>) is a fundamental metabolic requirement for heterotrophic marine  
34 organisms, excluding marine mammals (Portner, 2002; Keeling et al., 2010; Tiano et al., 2014).  
35 O<sub>2</sub> is declining due to warming, a tendency long predicted by models (Keeling et al., 2010; Long  
36 et al., 2016; Oschlies et al., 2018) and recently found evident at the global scale in compilations  
37 of in situ observations (Schmidtko et al., 2017; Ito et al., 2017). Deoxygenation is driven by the  
38 direct effect of reduced oxygen solubility with warming compounded by buoyancy-induced  
39 stratification in the upper ocean, which weakens the ventilation-mediated supply of fresh oxygen  
40 to the ocean interior. While the full ecological impacts of ocean deoxygenation remain uncertain,  
41 it is clear that the physiological impacts of oxygen loss on marine organisms can be considered  
42 explicitly in the context of warming: basal metabolic rates for ectothermic organisms depend on  
43 ambient temperature and increase with warming (Gillooly et al., 2001); thus, higher temperatures  
44 impose additional demand for oxygen to sustain aerobic respiration (Deutsch et al., 2015).  
45 Consequently, as the ocean warms, even present-day oxygen distributions may be insufficient to  
46 meet the oxygen demands of organisms living near key physiological thresholds (Deutsch et al.,  
47 2022).

48  
49 While model projections clearly demonstrate that warming and deoxygenation are consequences  
50 of human-driven climate change, it is important to recognize that natural climate variability also  
51 produces important fluctuations in these quantities. Indeed, evidence suggests that natural  
52 variability contributes to hypoxic events, such as those observed in the California Current, where  
53 fish and benthic-organism mortality has been associated with low-O<sub>2</sub> waters impinging on the  
54 continental shelf (Pozo Buil and Di Lorenzo, 2017; Howard et al., 2020). A clear understanding  
55 of how natural climate variability drives fluctuations in metabolic state and the associated  
56 implications for organisms is a critical context in which to view long-term climate warming.  
57 Given that the natural system is highly dynamic, climate change signals are often masked by  
58 decadal-scale variability (Ito and Deutsch, 2010). While numerous authors have considered  
59 detection and attribution of climate change for physical and biogeochemical variables (Rodgers  
60 et al., 2015; Long et al., 2016; Schlunegger et al., 2019), comparatively little attention has been  
61 devoted to explicitly characterizing the relative influence of natural and anthropogenic drivers of  
62 changes in the ocean's capacity to support aerobic life. In this study, we approach this challenge

63 by leveraging the concept of the Metabolic Index ( $\Phi$ ) introduced by Deutsch et al. (2015).  $\Phi$  is  
64 based on the notion that aerobic organisms can persist only where the ambient oxygen partial  
65 pressure ( $pO_2$ ) is sufficient to meet the requirements of sustaining respiration.  $\Phi$  incorporates an  
66 explicit representation of the dependence of metabolic oxygen demand on temperature, thus  
67 providing a framework to consider how joint oxygen and temperature variability constrain viable  
68 habitat in the ocean.

69

70 Many ocean organisms may already be under threat from deoxygenation (Hoegh-Guldberg and  
71 Bruno, 2010; Breitburg et al., 2018); however, ongoing climate-driven loss of oxygen raises  
72 important questions about the future of marine ecosystems: How will anthropogenic changes in  
73 dissolved oxygen and temperature impact the capacity of ocean habitats to support aerobic  
74 metabolism? What is the spatial and temporal distribution of changes in the ocean’s metabolic  
75 state associated with climate variability? At what point can anthropogenic change in the ocean’s  
76 metabolic state be distinguished from natural variability? This study addresses these questions  
77 using a combination of metabolic theory, a dataset set quantifying key physiological parameters  
78 for a collection of marine species adapted to specific environments (“ecotypes”), and the oxygen  
79 and temperature distributions simulated in the Community Earth System Model, version 1 Large  
80 Ensemble (CESM1-LE), which includes 34 members simulating ocean biogeochemistry under  
81 climate variability and change from 1920–2100 forced using historical data and the  
82 Representative Concentration Pathway Scenario 8.5 (RCP85) (Kay et al., 2015; Long et al.,  
83 2016).

84

85 This paper is organized as follows. Section 2 presents a brief overview of the relevant metabolic  
86 theory, the associated empirical datasets, and describes our approach to analysis. In Section 3 we  
87 present results quantifying the joint temperature-oxygen variability simulated in the CESM1-LE,  
88 evaluating the spatiotemporal structure of variability in marine ecotype habitat, including long-  
89 term trends based on the RCP8.5 scenario and time of emergence (ToE). The main outcomes of  
90 the results are synthesized in Section 4 and summarized in Section 5.

91

## 92 **2. Datasets and methods**

## 93 2.1 Metabolic index

94 Empirical studies measuring thermal tolerance and oxygen requirements in the laboratory on an  
95 array of marine organisms have enabled an assessment of lethal thresholds (Vaquer-Sunyer and  
96 Duarte, 2008; Rosewarne et al., 2016). These data coupled with recent advances in a theoretical  
97 framework enable both explanatory and predictive power in the context of a dynamic  
98 environment (Deutsch et al., 2015; Penn et al., 2018; Howard et al., 2020). The fundamental  
99 insights here are that basal metabolic rates for ectothermic marine organisms depend on ambient  
100 temperature and generally increase with warming (Gillooly et al., 2001). Increasing basal  
101 metabolic rates impose additional demand for oxygen. Organisms use oxygen dissolved in  
102 seawater and acquisition tends to be limited by diffusive processes; thus, oxygen supply is  
103 related to the ambient  $pO_2$ . The ratio of oxygen supply to temperature-dependent demand  
104 provides a critical indicator of the capacity for an organism to meet its metabolic requirements.  
105 Deutsch et al. (2015) formalized these concepts into a quantity termed the “Metabolic Index  
106 ( $\Phi$ )”, which is defined as the ratio of oxygen supply to an organism’s resting metabolic demand.  
107 Oxygen supply is parameterized according to a biomass-dependent scaling of  $pO_2$ , capturing  
108 variation in the efficiency with which organisms acquire and utilize  $O_2$ . This can be expressed as  
109  $S = \hat{\alpha}_s B^\sigma pO_2$ , where  $\hat{\alpha}_s$  represent gas transfer between an organism and its environment and  $B^\delta$   
110 is the scaling of supply with biomass,  $B$  (Piiper et al., 1971). Gas supply is represented as an  
111 Arrhenius function;

$$112 \quad \hat{\alpha}_s = \alpha_s \exp\left\{\frac{-E_s}{k_B} \left[\frac{1}{T} - \frac{1}{T_{ref}}\right]\right\} \quad (1)$$

113

114 Resting metabolic demand is also expressed using the Arrhenius equation as

$$115 \quad D = \alpha_D B^\delta \exp\left\{\frac{-E_d}{k_B} \left[\frac{1}{T} - \frac{1}{T_{ref}}\right]\right\}, \quad (2)$$

116 where  $\alpha_D$  is a species-specific basal metabolic rate,  $E_d$  (eV) is the temperature dependence of  
117 oxygen supply,  $T$  is temperature,  $T_{ref}$  is the reference temperature (15°C), and  $k_B$  is the  
118 Boltzmann constant (Gillooly et al., 2001). Gas transfer is kinematically slow at low  
119 temperatures, and hence organism viability can be limited by the energy to acquire oxygen at low  
120 temperatures, thus  $E_o$  varies with temperature. Here we account for this by adding the  
121 temperature dependence ( $dE_o/dT$ ) to  $E_o$  in equations above ( $E_o + \frac{dE_o}{dT}(T - T_{ref})$ ), using the mean

122 value of  $dE_o/dT = 0.022$  eV consistent with Deutsch et al. (2020). The Metabolic Index can thus  
 123 be written as the ratio of  $S/D$ :

$$\begin{aligned}
 124 \quad \Phi &= \frac{\alpha_s B^\sigma}{\alpha_D B^\delta} pO_2 \exp\left\{\frac{-E_s}{K_B} \left[\frac{1}{T} - \frac{1}{T_{ref}}\right] + \frac{E_d}{K_B} \left[\frac{1}{T} - \frac{1}{T_{ref}}\right]\right\}, \\
 125 \quad &= A_o B^{\sigma-\delta} pO_2 \exp\left\{\frac{E_d - E_s}{K_B} \left[\frac{1}{T} - \frac{1}{T_{ref}}\right]\right\}, \\
 126 \quad &= A_o pO_2 \exp\left\{\frac{E_o}{K_B} \left[\frac{1}{T} - \frac{1}{T_{ref}}\right]\right\}, \tag{3}
 \end{aligned}$$

127 where  $A_o = \alpha_s/\alpha_D$  ( $l/atm$ ) is the hypoxic tolerance,  $E_o = E_d - E_s$  ( $E_s$  is the temperature  
 128 dependence of oxygen supply) (Deutsch et al., 2015; Penn et al., 2018). The exponent,  $\varepsilon = \sigma -$   
 129  $\delta$ , is the allometric scaling of the supply to demand ratio with biomass, is typically near zero.  
 130 Therefore, in the analysis that follows, we presume unit biomass and thus neglect potential  
 131 impacts of variations in biomass.

132

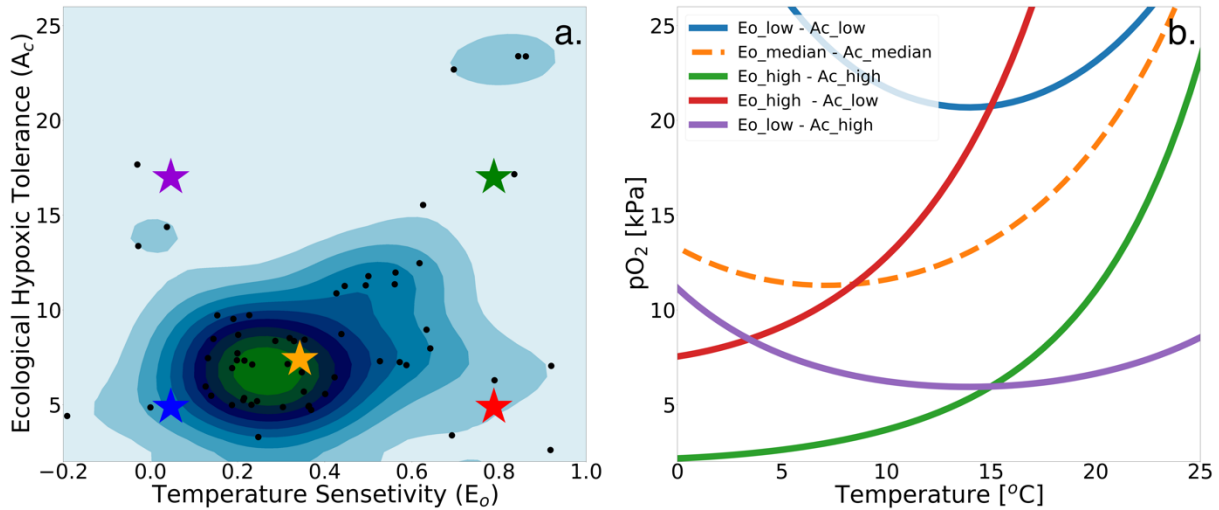
133 If  $\Phi$  falls below a critical threshold value of 1, conditions are physiologically unsustainable: an  
 134 organism cannot meet its basic resting metabolic oxygen requirements. Conversely, values of  $\Phi$   
 135 above 1 enable organismal metabolic rates to increase by a factor of  $\Phi$  above resting levels,  
 136 permitting critical activities such as feeding, defence, growth, and reproduction. Thus, for a  
 137 given environment and species,  $\Phi$  provides an estimate of the ratio of maximum sustainable  
 138 metabolic rate to the minimum rate necessary for basal metabolism. Deutsch et al. (2015)  
 139 inferred the ratio of active to resting energetic demand by examining the biogeographic  
 140 distribution of several species, finding that range boundaries coincide with values of  $\Phi = 1.5-7$ .  
 141 This threshold, termed critical rate ( $\Phi_{crit}$ ), represents the minimum metabolic index required for  
 142 an organism to sustain an active metabolic state, which is a more meaningful ecological  
 143 threshold than requirements for resting metabolism. Therefore, in this study, we define a quantity  
 144  $\Phi'$  derived by dividing  $\Phi$  by  $\Phi_{crit}$ , so when  $\Phi$  falls below 1, the organism can no longer sustain its  
 145 active metabolic demand and will need to make physiological trade-offs. Account for these  
 146 active metabolic requirements, we use an adjusted definition of the hypoxic tolerance trait,  $A_c =$   
 147  $A_o / \Phi_{crit}$ , where  $A_c$  is termed the “ecological hypoxia tolerance”, consistent with Howard et al.,  
 148 2020. Where  $\Phi' > 1$  (i.e.,  $\Phi > \Phi_{crit}$ ) an organism can sustain an active metabolic rate; where  $\Phi' <$   
 149  $1$  (i.e.,  $\Phi < \Phi_{crit}$ ),  $O_2$  is insufficient and an active metabolic state is not viable. Henceforth, our  
 150 analysis focuses on  $\Phi'$ ; in the subsequent  $\Phi' = \Phi$  for the text and figures.

151

## 152 **2.2 Physiological dataset**

153 We make use of a dataset describing physiological parameters for a collection of 61 marine  
154 ecotypes spanning a range of ecological hypoxic tolerances ( $A_c$ ) and temperature sensitivities  
155 ( $E_o$ ) (Penn et al., 2018; Deutsch et al., 2020, Figure 1a). The 61 species span benthic and pelagic  
156 habitats across four phyla in all ocean basins (Arthropoda, Chordata, Mollusca, and Cnidaria).  
157 The dataset include 28 malacostracans, 21 fishes, three bivalves and cephalopods, two copepods,  
158 and one each for gastropods, ascidians, scleractinian corals, and sharks with body mass spans of  
159 eight orders of magnitude (Penn et al., 2018). We illustrate how the physiological traits  $E_o$  and  $A_c$   
160 constrain habitat viability in the context of distributions of  $pO_2$  and temperature in the marine  
161 environment in Figure 1b, which shows the minimum  $pO_2$  (i.e.,  $pO_2$  at  $\Phi_{crit}$ ) required to sustain  
162 an active metabolic state as a function of temperature for five combinations of  $E_o$  and  $A_c$ . The  
163 five combinations are derived from sampling the probability distributions of  $E_o$  and  $A_c$  (Figure  
164 1a) at the 10<sup>th</sup>, 50<sup>th</sup>, and 90<sup>th</sup> percentile values (illustrated by colored stars in Figure 1a and  
165 corresponding curves in Figure 1b). We assume that the trait distributions are independent, which  
166 is a reasonably modest simplification;  $E_o$  is represented by a normal distribution and  $A_c$  by a  
167 lognormal distribution function (Figure S1). The  $pO_2$  at  $\Phi_{crit}$  curves shown in Figure 1b delineate  
168 regions of  $pO_2$ -temperature space that are habitable (above the curve) and uninhabitable (below  
169 the curve). The reversing curvature of  $pO_2$  at  $\Phi_{crit}$  in Figure 1b at low temperature captures the  
170 decrease of the organism's oxygen acquisition efficiency in cooler conditions yielding cold  
171 intolerance. At very low temperatures, gas transfer is limited by the decrease in molecular gas  
172 diffusion, as a consequence, oxygen transfer into the organisms requires energy, yielding cold

173 intolerance, this is well illustrating by the blue line in Figure 1b.



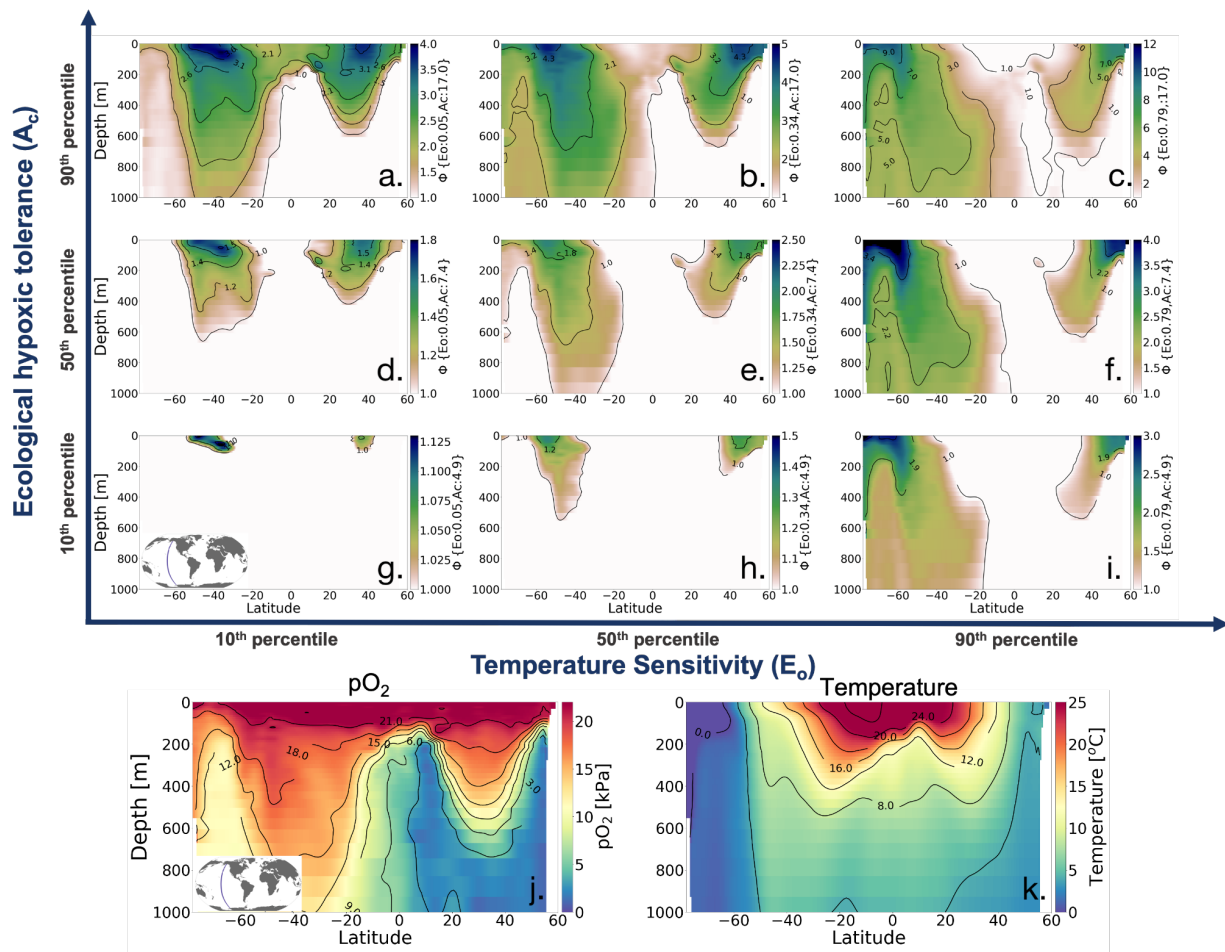
174

175 **Figure 1.** Physiological traits determining hypoxic tolerance. (a) Scatter plot of 61 marine ecotypes for which  
176 empirically derived estimates of activation energy ( $E_o$ ) and the ecological hypoxic tolerance ( $A_c$ ) have been  
177 determined (Penn et al., 2018). The color shows the density of occurrence for the 61 marine ecotypes in the  $A_c - E_o$   
178 trait space. (b) The minimum  $pO_2$  required to sustain an active metabolic state (i.e.,  $pO_2$  at  $\Phi_{crit}$ , Deutsch et al., 2020)  
179 for five combinations of  $A_c$  and  $E_o$  corresponding to the stars in panel “a”; these are combinations of the 10th, 50th,  
180 90th percentile values for each parameter. Below the  $pO_2$  lines shown, the organism would experience an oxygen  
181 deficit relative to its active metabolism requirements, effectively signifying the species-specific hypoxic conditions,  
182 based on physiological traits, for this range of temperatures.

183

184 To illustrate how the trait combinations of  $E_o$  and  $A_c$  exert control on the geographic distribution  
185 of organisms in the marine environment (Deutsch et al., 2020), we use observations of  $pO_2$  and T  
186 along a zonal transect of the Pacific Ocean and plot  $\Phi'$  for nine combinations of  $E_o$  and  $A_c$   
187 percentile values (Figure 2). The colorbar in Figures 2a-i show the metabolic index for an active  
188 state ( $\Phi'$ ); regions with values above one are habitable (color), while regions with values below  
189 one are uninhabitable (white) on the basis of metabolic constraints (other ecological  
190 considerations are not considered). The subplots in the upper portion of the figure are arranged  
191 according to the same trait axes shown in Figure 1a;  $E_o$  increases horizontally from left to right  
192 and  $A_c$  increases from the bottom to the top. For the trait combination in the bottom left (low  $E_o$ ,  
193 low  $A_c$ ; Figure 2g), metabolism is relatively insensitive to temperature, and tolerance for low  
194  $pO_2$  is poor. Thus, ecotypes with low  $E_o$  and low  $A_c$  are restricted to high latitude surface waters,  
195 where temperatures are cool, and  $pO_2$  is abundant (Figure 2g). As  $E_o$  increases from left to right,

196 metabolic rates become more sensitive to temperature. Then, habitat is gained at depth, where  
 197 temperatures are cooler and higher temperature sensitivity confers an advantage (Figure 2g–i).  
 198 From the bottom to the top, the increase in tolerance of low  $pO_2$  conditions increases habitability  
 199 in regions of low  $pO_2$ , enabling organisms to expand beyond high-latitude surface waters (Figure  
 200 2g-a). The biogeographic range for organisms with high  $A_c$  is modulated by  $E_o$ ; as temperature  
 201 sensitivity increases, ecotype viability at high latitudes is increased, but tropical surface waters  
 202 become less viable (Figure 2 a-c). Henceforth, our analysis will utilize the metabolic index of the  
 203 median ecotype ( $E_o = 0.34$ ,  $A_c = 7.4$ ; Figure 2e) for illustrative purposes; i.e., all metabolic index  
 204 figures refer to this median ecotype unless otherwise stated.



205  
 206 **Figure 2.** Annual mean metabolic index ( $\Phi$ ) for nine combinations of the ecological traits  $E_o$  (metabolic  
 207 temperature sensitivity) and  $A_c$  (ecological hypoxic tolerance) along a transect in the Pacific Ocean based on a  
 208 climatology from the World Ocean Atlas dataset (Garcia et al., 2014). The percentile values of each trait are: 10<sup>th</sup> ( $E_o$   
 209 = 0.04,  $A_c = 4.8$ ), 50<sup>th</sup> ( $E_o = 0.34$ ,  $A_c = 7.4$ ), and 90<sup>th</sup> ( $E_o = 0.79$ ,  $A_c = 17.0$ ). The lower panels show  $pO_2$  and



210 temperature from the WOA dataset. Note that the colorbar range differs by panel and values where  $\Phi' < 1$  are  
211 omitted, thus the color shows only areas where an active metabolic state can be sustained.

212

### 213 **2.3 Earth system model simulations**

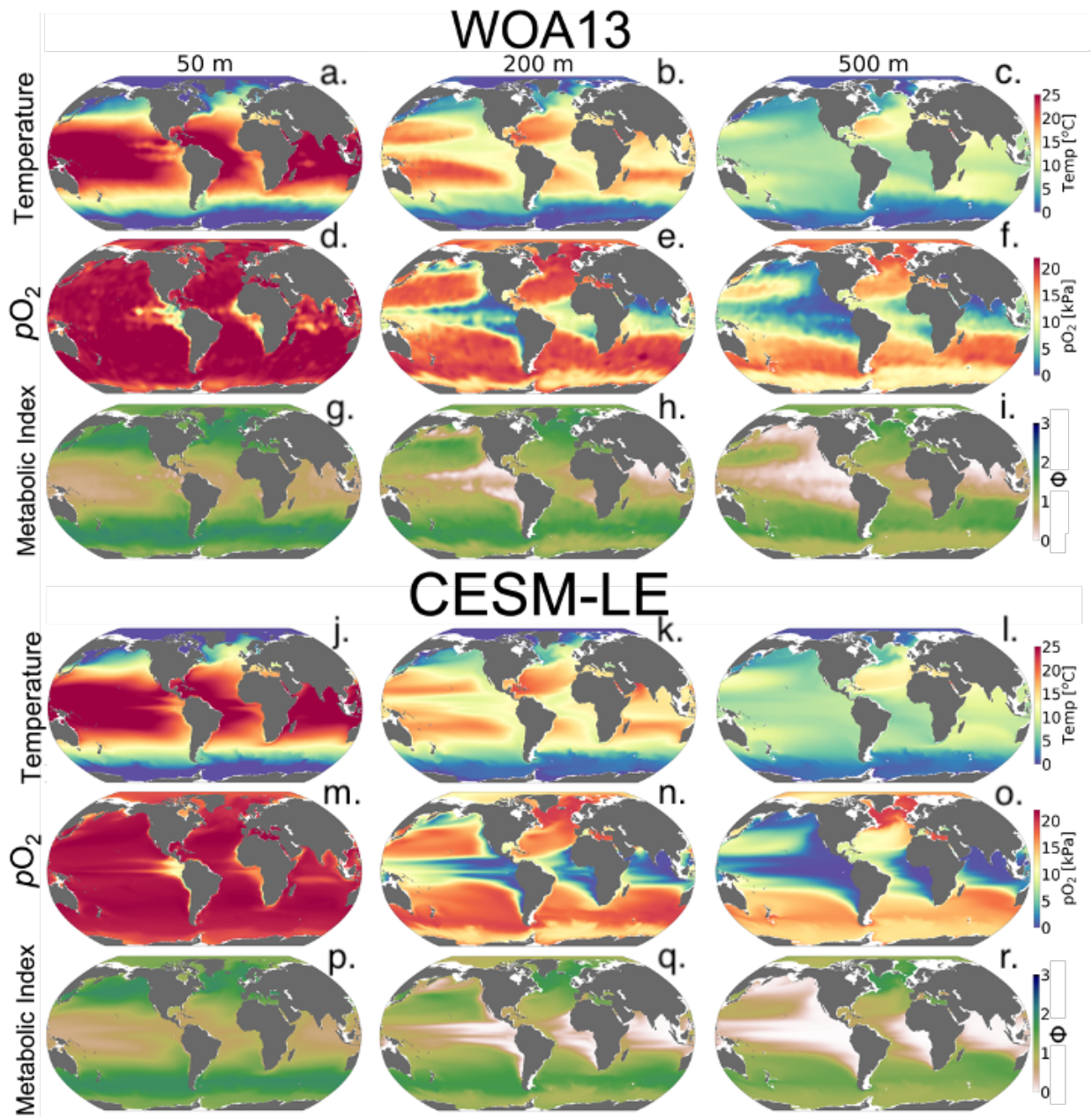
214 This study is based on the CESM1-LE, described in detail by Kay et al. (2015). The CESM1-LE  
215 included 34 ensemble members integrated from 1920–2100 under historical and RCP8.5 forcing.

216 The ensemble was generated by adding round-off level ( $10^{-14}$  K) perturbations to the air  
217 temperature field at initialization in 1920; this small difference yields rapidly diverging model  
218 solutions due to the chaotic dynamics intrinsic to the climate system, thus developing ensemble  
219 spread representative of internal variability (Kay et al., 2015). Briefly, the CESM1-LE uses the  
220 Community Earth System Model, version 1 (Hurrell et al., 2013), with a horizontal resolution of  
221 nominally  $1^\circ$  in all components. The ocean component is Parallel Ocean Program version 2,  
222 (Smith et al., 2010) with sea ice simulated by the Los Alamos Sea Ice Model version 4 (Hunke  
223 and Lipscomb, 2010). Ocean biogeochemistry was represented by the Biogeochemical Elemental  
224 Cycling (BEC) model (Moore et al., 2013; Lindsay et al., 2014).

225

226 Our analysis focuses on three depths: 50 m representing near-surface dynamics, the epipelagic  
227 zone at 200 m, and the mesopelagic zone at 500 m.  $pO_2$  was calculated using the Garcia and  
228 Gordon. (1992) solubility formulation. For convenience, we use the period 1920–1965 to define  
229 a minimally-perturbed natural state, as this period is prior to the development of substantial  
230 anthropogenic trends in ocean oxygen and temperature (Long et al., 2016). We also examine  
231 distributions over the last three decades of the 21st century (2070–2099) to evaluate the projected  
232 climate-change signal under RCP8.5. We use the mean across all 34 ensemble members to  
233 quantify the deterministic, “forced” response of the climate system to anthropogenic influence  
234 (Deser et al., 2012). The ensemble spread is thus indicative of the amplitude of variations  
235 attributable to natural variability.

236



237  
 238 **Figure 3.** Mean-state comparison with observations. The climatological mean of (top rows) temperature (°C),  
 239 (middle rows)  $pO_2$  (kPa), and the (bottom rows) metabolic index for active metabolism ( $\Phi$ ) for the median ecotype  
 240 ( $E_o = 0.34$ ,  $A_c = 7.4$ ); three depths are shown (left) 50 m, (center) 200 m, and (right) 500. Top panels show the  
 241 WOA13 dataset and the bottom panels show CESM1-LE.

242  
 243 We compared the CESM1-LE (1920 - 1965) with the World Ocean Atlas, version 2013  
 244 (WOA2013) dataset (Garcia et al., 2014), an observationally-based, gridded climatology (Figure  
 245 3a-i). CESM1-LE generally provides a reasonable representation of  $pO_2$  and temperature

246 distributions at the selected depths (Figure 3); however, there are important biases to  
247 acknowledge in the context of interpreting the results. Temperature magnitudes are generally  
248 well simulated in the CESM1-LE, showing a root mean square error (RMSE)  $< 1.3$  °C, and  
249 pattern correlation coefficient (PCC)  $> 0.98$  in all three selected depths (50 m, 200 m, and 500)  
250 (Table 1). Temperature magnitudes are slightly underestimated at 50 m and 200 m (mean bias of  
251  $< 0.3$ °C), and overestimated by  $0.41$  °C at 500 m. Note that since our comparison uses CESM1-  
252 LE data from 1920-1965, some discrepancy in temperature might be expected from the signal of  
253 climate warming present in the WOA observations.  $pO_2$  is also reasonably well captured by the  
254 CESM1-LE (PCC  $< 0.95$ ), but magnitudes are slightly underestimated at depth, showing a mean  
255 bias of  $-1.63$  kPa and  $-2.1$  kPa at 200 m and 500 m with respect to WOA13 (Table 1). Regions of  
256 low  $pO_2$  waters are too extensive in CESM1-LE (Figure 3n-o) and there is a slight degradation of  
257 skill with depth for  $pO_2$  fields (Table 1). The underestimation of  $pO_2$  leads to a slight  
258 underestimation of  $\Phi'$  with respect to WOA13, and overestimate habitat loss in the future  
259 climate (Figure 3 p-r); however,  $\Phi'$  computed from the model fields demonstrates that the  
260 dominant spatial patterns are well captured by the CESM1-LE despite magnitudes that are  
261 slightly too low (i.e., Figure 1, c, l). This CESM  $pO_2$  bias is common among coarse-resolutions  
262 ocean models and it is attributed to a sluggish circulation and hence weak ventilation (Long et  
263 al., 2016). These differences ultimately matter most near the hypoxic zones and at the boundaries  
264 of habitable zones like the Oxygen Minimum Zones (OMZs).  
265  
266

267 **Table 1.** Summary statistics for the comparison of CESM1-LE with the World Ocean Atlas dataset (Garcia et al.,  
 268 2014). The columns include the mean bias, pattern correlation coefficient (PCC), and root mean square error  
 269 (RMSE) at 50 m, 200 m, and 500 m.

	<b>Mean bias</b>	<b>R</b>	<b>RMSE</b>
	<b>Temperature [°C]</b>		
<b>50 m</b>	-0.17	0.99	1.22
<b>200 m</b>	-0.25	0.99	1.22
<b>500 m</b>	0.10	0.98	0.63
	<b>pO<sub>2</sub> [kPa]</b>		
<b>50 m</b>	0.05	0.99	1.91
<b>200 m</b>	-1.17	0.96	5.96
<b>500 m</b>	-1.46	0.95	6.28
	<b>Metabolic index</b>		
<b>50 m</b>	0.01	0.99	0.02
<b>200 m</b>	-0.09	0.97	0.05
<b>500 m</b>	-0.15	0.96	0.08

270

271

## 272        2. Results

273

### 274            3.1 Joint temperature- $pO_2$ natural variability and forced trends

275

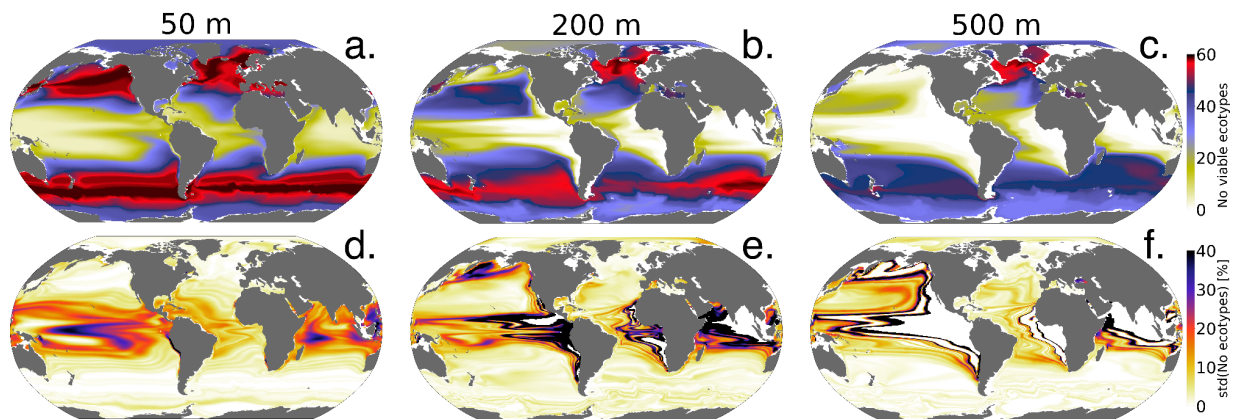
276 The spatial distribution of the number of viable ecotypes is shown in Figure 4 for the  
277 “unperturbed” climate (1920-1965). Our intention here is not to quantify the actual  
278 biogeographic range of organisms in the environment, but rather to illustrate the ocean’s ability  
279 to support respiration by marine ectotherms given the metabolic capacities afforded within the  
280 trait space of extant organisms. High latitude environments do not impose strong aerobic  
281 constraints (cold intolerance notwithstanding), thus over much of the Southern Ocean, North  
282 Atlantic, and Arctic Ocean almost all 61 ecotypes can sustain respiration. The tropical oceans  
283 impose the strongest aerobic constraints, restricting the viability of ecotypes that do not have  
284 high-hypoxia tolerance ( $A_o$ ). For example, less than 25 ecotypes are viable over much of the  
285 tropical surface ocean (Figure 4a); low concentrations of oxygen at depth impose even stronger  
286 constraints, and no ecotypes are viable in the core of OMZs (Figure 4b, c). The spatial patterns of  
287 the number of viable ecotypes is tightly controlled by temperature at the surface, since  $pO_2$  is  
288 mostly near saturated levels; at depth, however,  $pO_2$  is the dominant driver of geographic  
289 patterns in ecotype viability (Figures 2-4). Temperature generally decreases with depth, reducing  
290 the metabolic oxygen demand. However, since  $pO_2$  also decreases with depth and displays  
291 greater lateral heterogeneity,  $pO_2$  emerges as the dominant constraint of spatial structure in  
292 ecotype viability at depth.

293

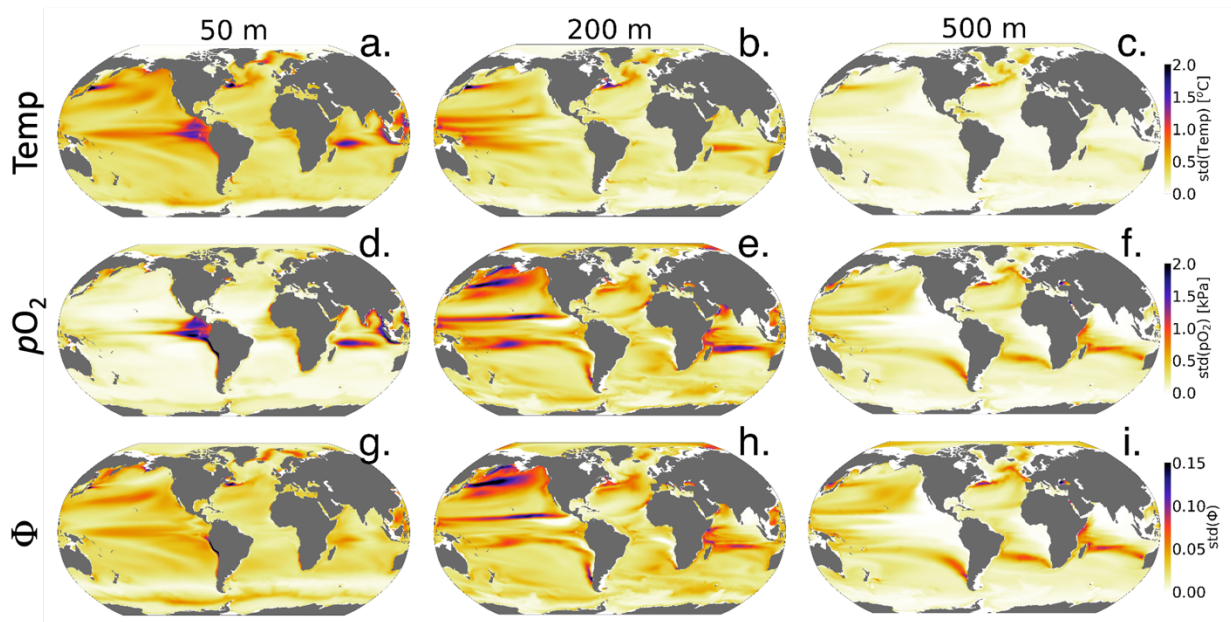
294 The standard deviation of annual anomalies using all CESM1-LE ensemble members provides  
295 insight into the amplitude of natural variability (Figure. 5, one standard deviation). Temperature  
296 and  $pO_2$  show similar patterns of natural variability in the upper ocean, both showing particularly  
297 large variance in the western tropical Pacific and Indian Ocean (Figure 5 a, d). Spatial variation  
298 in the magnitude of temperature variability generally decreases with depth, but  $pO_2$  displays even  
299 relatively larger variability at depth with respect to the surface in some regions (Figure 5 a–f).

300 The joint  $pO_2$ -temperature variability manifests in variations of  $\Phi'$  (Figure 5g-i). Natural  
301 variability in  $\Phi'$  computed for the median ecotype shows spatial patterns similar to temperature

302 in the upper-surface ocean (50 m), but is more similar to  $pO_2$  at depth. Thus, variations in  $\Phi'$  tend  
 303 to be temperature-dominated near the surface, but are more strongly controlled by  $pO_2$  variability  
 304 at depth.  $\Phi'$  also shows the most extensive natural variability at 200 m consistent with the  
 305 variability of  $pO_2$ . The number of viable species shows more dramatic fluctuations than  
 306 variations in the median ecotype  $\Phi'$ ; variations in the number of viable ecotypes exceed 30% on  
 307 annual timescales in the tropical upper ocean and near OMZ boundaries in the water column  
 308 (Figure 4 c–d). This reflects the fact that interannual variability can preclude habitability for  
 309 some regions of the  $A_c$ - $E_o$  trait space, but these variations do not necessarily impact viability for  
 310 the median ecotype (Figure 1). In the tropical surface ocean, high temperatures ( $>25^\circ\text{C}$ ), and  
 311 saturated surface ( $pO_2 > 20$  kPa) require high hypoxia tolerance ( $A_c$ ), but permit a range of  
 312  $E_o$  values (Figure 1b, 2a-b). Ecotypes with larger temperature sensitivity (high  $E_o$ ) are  
 313 particularly responsive to variations in temperature.  
 314



315  
 316 **Figure 4.** Metabolic constraints on trait-space viability. Top row: the number of ecotypes from the physiological  
 317 trait database that are viable (total = 61) in the CESM1-LE over the period 1920–1965. Bottom row: the standard  
 318 deviation (expressed as a percent of the mean) in the number of viable ecotypes, reflecting fluctuations driven by  
 319 natural variability.  
 320

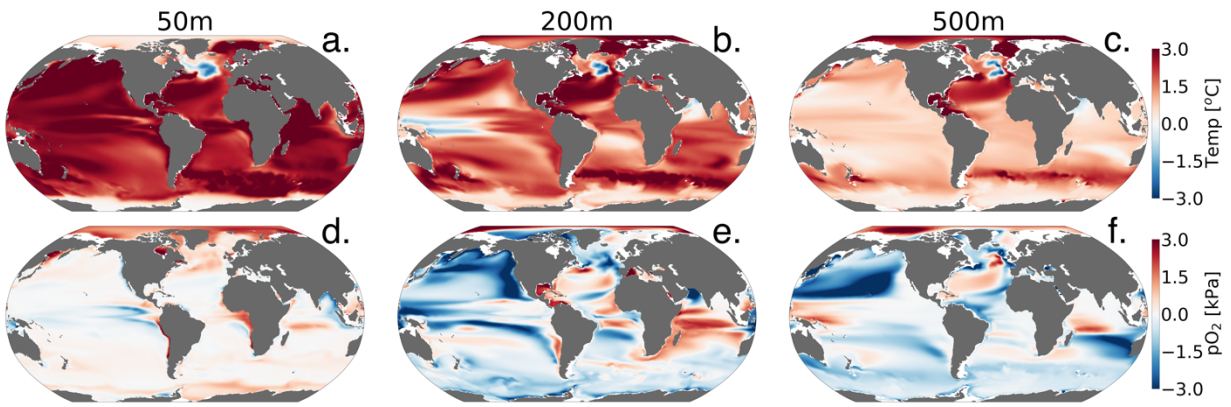


321  
 322 **Figure 5.** The amplitude of natural variability in the ocean’s metabolic state. The panels show the standard deviation  
 323 of annual-mean anomalies of all ensemble members over the period 1920–1965 for (top row) temperature (°C),  
 324 (middle row)  $pO_2$  (kPa), and (bottom row) the metabolic index (unitless) of the median ecotype ( $E_o = 0.34$ ,  $A_c = 7.4$ ).  
 325

326 CESM1-LE simulates nearly homogeneous warming between 1920–1965 and 2070–2099 in the  
 327 surface ocean (50 m) under RCP8.5, with an exception of the so-called North Atlantic warming  
 328 hole (Figure 6a). Both modelling and observational studies have linked the North Atlantic  
 329 warming hole to the slowing of the Atlantic overturning circulation with climate change (Keil et  
 330 al., 2020). The magnitude of ocean warming generally diminishes with depth except in the North  
 331 Atlantic, where, despite reductions, the overturning circulation effectively propagates  
 332 anthropogenic heat anomalies into the ocean interior.  $pO_2$  shows heterogeneous changes between  
 333 1920–1965 and 2070–2099 (Figure 6 d-f). In the upper ocean,  $pO_2$  changes are generally small (<  
 334 1 kPa) because the near-surface is kept close to saturation via photosynthetic oxygen production  
 335 and air-sea equilibration. At depth, however,  $pO_2$  shows long-term changes linked to  
 336 accumulated effects of respiration and changes in circulation (Ito et al., 2017). At 200 m for  
 337 example, the Pacific Ocean displays a basin-wide mean reduction in  $pO_2$  of 2 kPa (~30%), while  
 338 the Atlantic and Indian basins gain about >2 kPa (~ 10 - 35%) by the end of the century. The  
 339 largest long-term  $pO_2$  loss (>3 kPa) occurs in the North Pacific while the largest  $pO_2$  gain (~2



340 kPa) occurs in the North Atlantic gyre and western Indian Ocean (Figure 6 e-f).

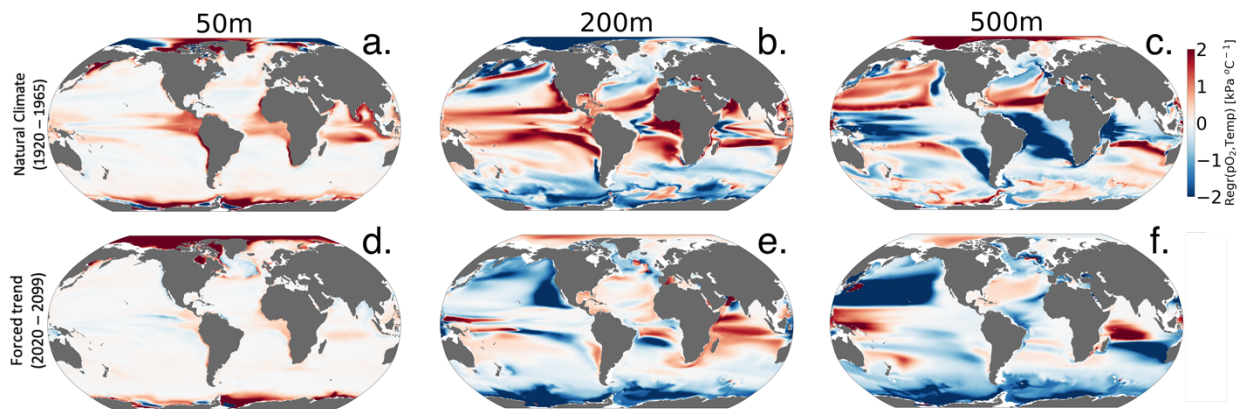


341  
342 **Figure 6.** Net long-term change (2070–2099 minus 1920–1965) in the CESM1-LE ensemble means temperature  
343 (top) and (bottom)  $pO_2$  at 50 m, 200 m, and 500 m.

344  
345 Figure 7 shows the relationship between interannual variations in  $pO_2$  versus temperature ( $pO_2$ -  
346 T) in the unperturbed climate (1920–1965; top row) and for the forced trend associated with 21st  
347 century climate change (2070–2099 minus 1920–1965; bottom row). The nature of the  $pO_2$ -T  
348 relationship is an important indicator of the impacts of variability on the metabolic state.  
349 Furthermore, the extent to which the forced trend is characterized by a  $pO_2$ -T relationship that is  
350 distinct from that associated with natural variability provides insight into the potential for  
351 advanced or delayed detection of signals in  $\Phi$  relative to  $pO_2$  or temperature alone. Given that  
352 metabolic rates for most organisms increase with temperature (positive  $E_o$ ), a positive correlation  
353 between variations in temperature and  $pO_2$  is generally indicative of compensating changes,  
354 wherein increased oxygen demand is at least partially offset by increased supply. Anticorrelation  
355 between temperature and  $pO_2$ , by contrast, will generally be associated with compounding  
356 impacts on the metabolic index, as a negative correlation indicates that reductions in  $pO_2$  (i.e.,  
357 oxygen supply) accompany warming (i.e., increased demand). The sign of the  $pO_2$ -T relationship  
358 in the natural climate varies regionally and with depth (Figure 7, top row). The surface ocean is  
359 generally characterized by a weak, positive  $pO_2$ -T relationship, which could manifest from,  
360 among other mechanisms, temperature-induced increases in photosynthetic oxygen production  
361 (Figure 7a). The natural  $pO_2$ -T relationship in the epipelagic (200 m) is characterized by strong  
362 positive correlations in the tropics and negative correlations at high latitudes (Figure 7b). A  
363 positive correlation between  $pO_2$  and temperature at this depth could be induced by variability



364 associated with adiabatic vertical displacement of isopycnals, or “heave”, which has the effect of  
 365 translating background gradients in properties vertically in the water column (Long et al., 2016).  
 366 Upward movement of a deep isopycnal surface would yield a negative temperature anomaly and  
 367 a negative  $pO_2$  anomaly (positive correlation), as the deeper, colder waters have greater oxygen  
 368 utilization signatures associated with longer ventilation age. Negative correlations between  $pO_2$   
 369 and temperature could manifest from ventilation processes, where enhanced subduction of  
 370 surface water yields anomalously cold water masses that are enriched in oxygen. The sign of  
 371 these epipelagic  $pO_2$ -T correlations shows some similarity to those associated with the externally  
 372 forced climate (Figure 6e), but the latter is characterized by a greater prevalence of  
 373 anticorrelation, most notably in the North Pacific ocean. At 500 m depth, the relationship  
 374 between temperature and  $pO_2$  in the natural climate is almost a mirror image of the epipelagic  
 375 (Figure 7c); the tropics generally display negative correlations, while polar regions show positive  
 376 correlations (Figure 7 e). The  $pO_2$ -T relationship in the forced trend at 500 m is dominated by  
 377 broad regions of deeply negative correlations, with the most pronounced effect again in the  
 378 North Pacific. The negative relationship is consistent with a ventilation signal, as buoyancy-  
 379 induced stratification from warming curtails the introduction of new oxygen into the ocean  
 380 interior. The predominantly negative  $pO_2$ -T relationship associated with the forced trend is  
 381 indicative of the compounding effects of climate change on metabolic state, increasing metabolic  
 382 demand while simultaneously reducing oxygen supply.



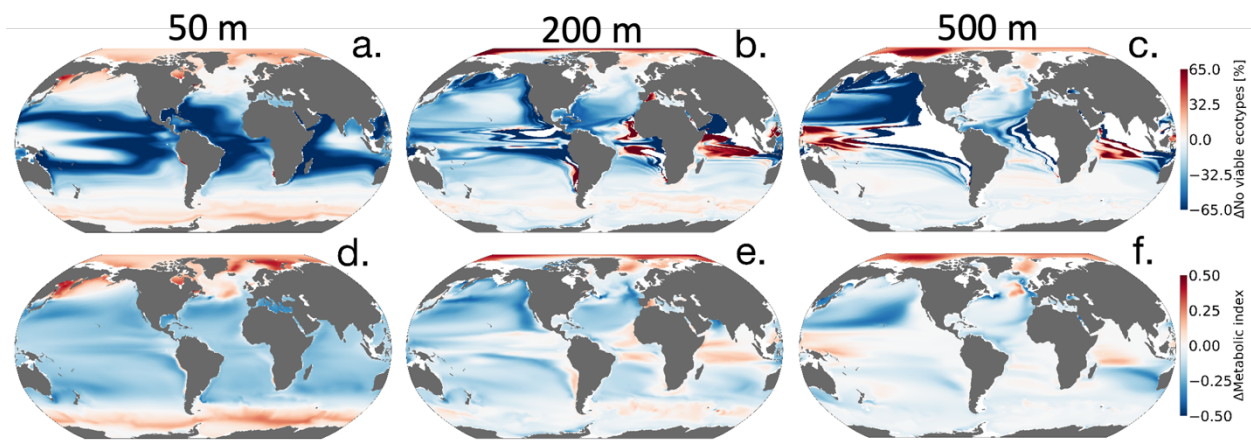
383  
 384 **Figure 7.** Regression of annual means  $pO_2$  versus temperature ( $kPa \text{ } ^\circ C^{-1}$ ) for (top row) interannual variability and  
 385 (bottom row) the forced trend (difference between 2020–2099 and 1920–1965). The columns show the regressions  
 386 computed at different depths, 50 m, 200 m, and 500 m, respectively.

387

### 388 3.2 Long-term habitat changes

389

390 Figure 8 shows the climate-driven changes in  $\Phi'$  for the median ecotype, as well as the impacts  
391 of climate change on the number of viable ecotypes. Notably, while  $pO_2$  in the near-surface  
392 ocean is relatively insensitive to climate change (Figure 6d), there are reductions in  $\Phi'$  in the  
393 tropics (Figure 9d), owing to the direct impacts of warming. These changes are associated with  
394 deep reductions in the number of viable ecotypes in the tropics (Figure 8a). There are modest  
395 increases in  $\Phi'$  and ecotype viability at high-latitudes; metabolic state in these regions is affected  
396 by cold intolerance, thus warming broadens the viable region of trait space. Additionally,  
397 reductions in sea ice cause an increase in  $pO_2$ , as gas exchange becomes more effective at  
398 restoring equilibrium oxygen concentrations. The number of viable ecotypes shows more intense  
399 patterns than those in the median ecotype  $\Phi'$  in the upper ocean (Figure 8). This is partly because  
400 ecotypes predicted to lose viability in the tropical regions ( $\sim 50\%$ ) are at the extremes of the  $A_c$ -  
401  $E_o$  distribution (Figure 1) and not captured by the median ecotype  $\Phi'$ . Nevertheless, outside the  
402 tropical regions, the median ecotype gives a good indication of the anthropogenic impact to  
403 marine ectotherms. The projected habitat loss in the epipelagic-pelagic North Pacific ( $> 50\%$ )  
404 and habitat gain in the epipelagic-pelagic Southern Indian Ocean ( $\sim 40\%$ ) and pelagic western  
405 tropical regions ( $\sim 40\%$ ) are consistent with a decrease in the median ecotype  $\Phi'$ . Note that the  
406 most pronounced effects on habitat are associated with regions where climate change drives a  
407 strongly negative  $pO_2$ -temperature relationship (Figure 7).



408

409 **Figure 8.** Net change in the number of habitable ecotypes in percentage (top row). Net metabolic index change

410 (2070 - 2099 vs. 1920 - 1965) for the median ecotype [ $E_o = 0.34$ ,  $A_c = 7.4$ ] (bottom row). At 50m (first column),  
411 200m (second column) and 500m (third column).

412

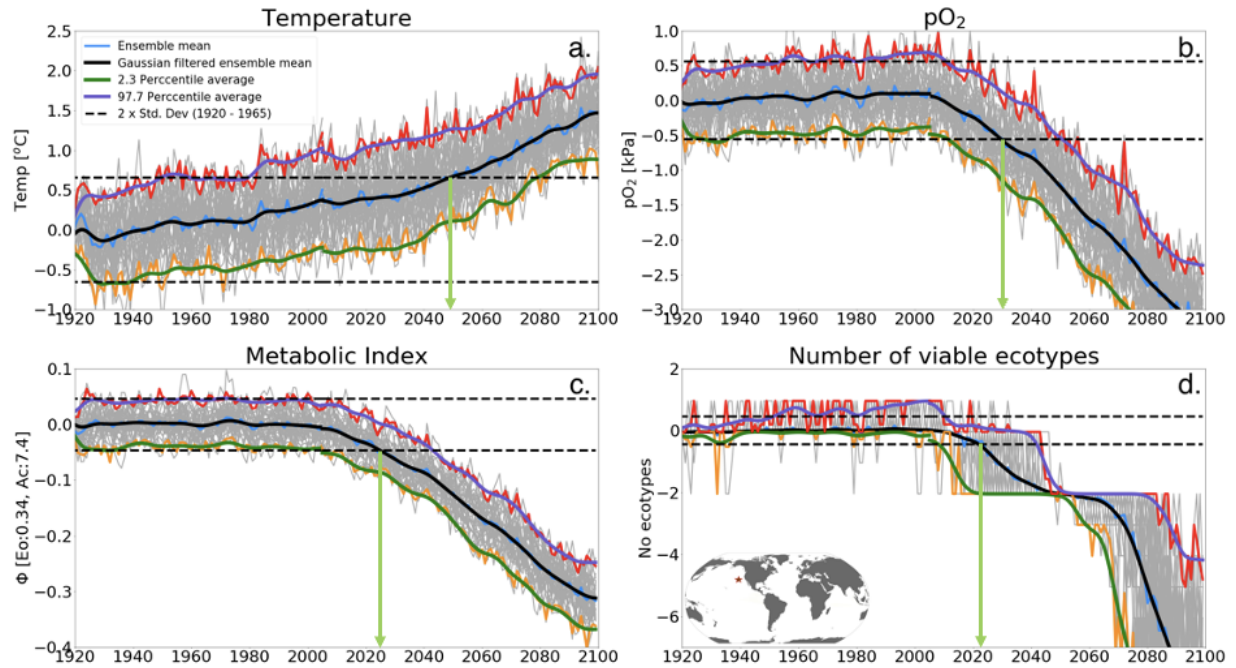
### 413 **3.3 Time of Emergence**

414

415 In this section, we examine the “time of emergence” (ToE, Hawkins and Sutton, 2012), the point  
416 when forced changes in  $pO_2$ , temperature and  $\Phi'$  can be distinguished from the background  
417 natural variability. We define ToE as the time when the magnitude of change in the ensemble  
418 mean of a particular variable exceeds two standard deviations of the natural climate (1920 -  
419 1965). This is illustrated in Figure 9 for a single grid point in the North Pacific at 200 m. At this  
420 location, the forced trend in temperature shows a monotonic increase, while  $pO_2$  shows a  
421 monotonic decrease; as a result,  $\Phi'$  for the median ecotype and the number of viable ecotypes  
422 decrease over time. The anti-correlation between  $pO_2$  and temperature exacerbates trends in  $\Phi'$ ,  
423 and hence the forced trend of the median ecotype  $\Phi'$  emerges from natural noise earlier than  
424 either  $pO_2$  or temperature do alone (Figure 10a-c). Note that although the ToE of ecotype  
425 viability change is directly derived from changes in  $\Phi'$ , it is binary counted; changes in ecotype  
426 viability are counted in whole numbers and this creates a step-function temporal-spatial variation  
427 (Figure 9d). Consequently, this step-function-like feature of ecotype viability creates  
428 discontinuities even in spatial patterns of ToE (Figure 10 j-l) as also shown in the natural  
429 variance in Figure 4 d-f.

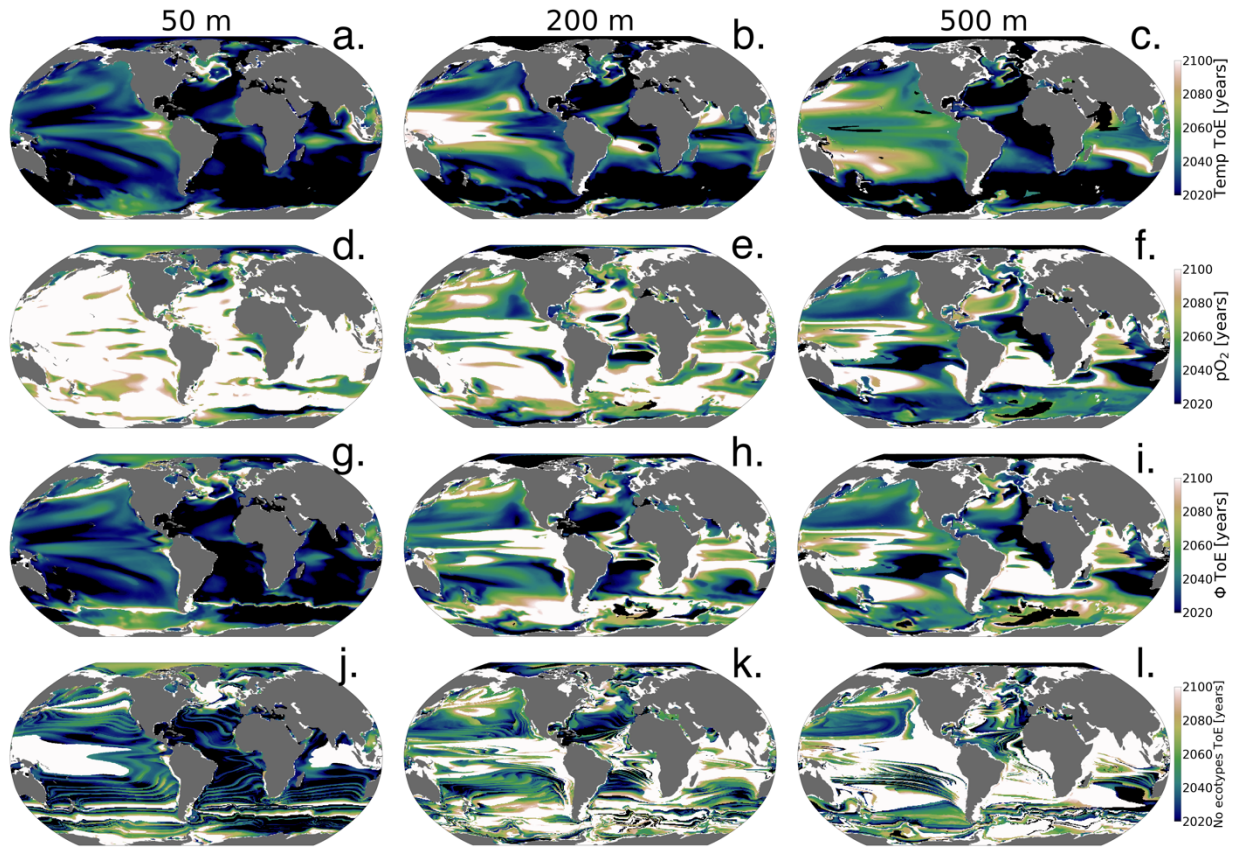
430

431



432  
 433  
 434  
 435  
 436  
 437  
 438

**Figure 9.** Time of emergence (ToE) of the climate forcing signal for (a) temperature, (b)  $pO_2$  (c) the metabolic index of the median ecotype [ $E_o = 0.34$ ,  $A_c = 7.4$ ], and (d) the number of viable ecotypes for a single model grid in the North Pacific at 200 m. ToE (green arrows) is defined as the time when the forced trend signal (ensemble member time series) is above two standard deviations (black dotted line) of all ensemble members for the period 1920 - 1965.



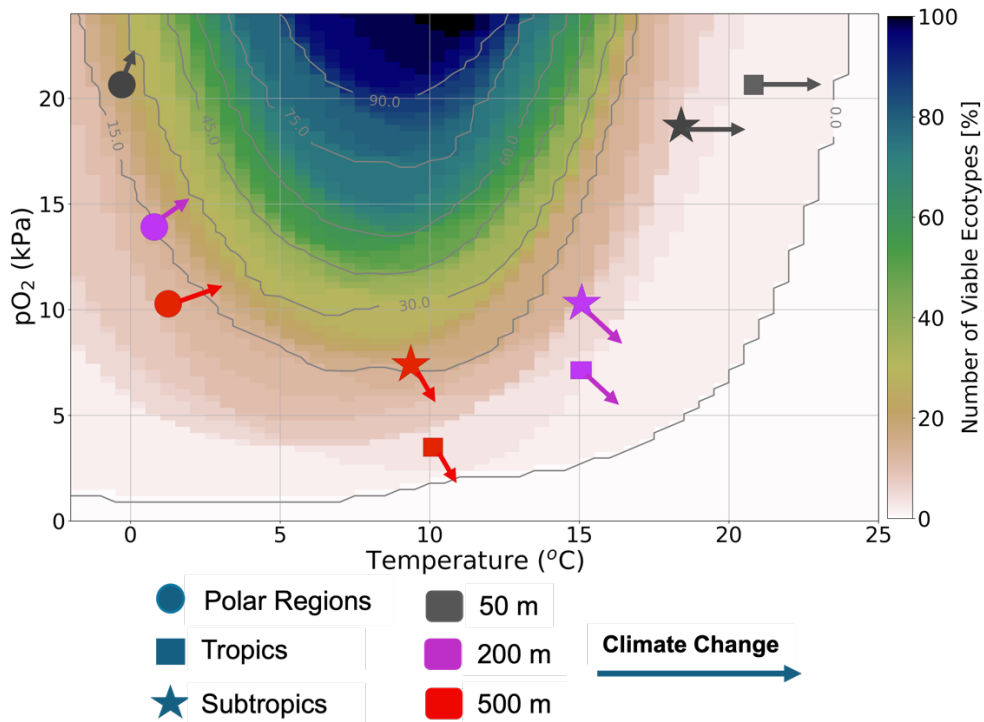
439  
 440 **Figure 10.** Time of emergence (ToE) of the climate forcing signal for temperature,  $pO_2$ ,  $\phi$ , and the number of  
 441 viable ecotypes. ToE is defined as the time when the forced trend signal (ensemble member time series) is above  
 442 two standard deviations of all ensemble members for the period 1920 - 1965.

443  
 444 The ToE of  $pO_2$  and temperature are inverted with depth; temperature emerges earliest in the  
 445 upper ocean while  $pO_2$  emerges earlier at depth and later or shows no emergence in the upper  
 446 ocean (Figure 10 a-f). This feature is consistent with larger upper ocean temperatures long-term  
 447 changes and greater  $pO_2$  changes at depth. Near-surface ocean temperature has mostly already  
 448 emerged by 2020 and is predicted to have almost completely emerged by the late 2060s under  
 449 RCP85 (Figure 10 a-c). The early emergence of temperature from natural noise also persists for  
 450 regions of relatively low natural variance at depth, e.g., the Southern Ocean and Atlantic Basin  
 451 Gyres. Regions of the largest natural variability (see Figure 5) like the subtropical-subpolar  
 452 Pacific however do not emerge until close to the end of the century. For  $pO_2$ , anthropogenic  
 453 changes in the upper ocean generally do not emerge from natural noise before the end of the  
 454 century except for the Arctic Ocean and Eastern Antarctic. In the Arctic Ocean and Eastern



455 Antarctic  $pO_2$  gain is related to sea-melt emergence by the mid-2050s (Figure 10a). The median  
456 ecotype  $\Phi'$  ToE shows spatial patterns that are coherent with temperature ToE in the upper ocean  
457 with exception of polar regions. In contrast, they are consistent with  $pO_2$  ToE patterns at depth;  
458 this is consistent with net long-term  $\Phi'$  changes in Figure 9d. The emergence of the  
459 anthropogenic signal in ecotype viability closely resembles the median ecotype  $\Phi'$  spatial  
460 patterns but showing non-harmonious spatial patterns due to the step-function-like counting  
461 feature of viability changes. It shows that the predicted  $\sim 50\%$  ecotype viability loss in the  
462 tropics (Figure 6a) may already be distinguishable from natural variability by the mid-2030s. In  
463 the North Pacific, the predicted  $> 50\%$  ecotype viability loss in the epipelagic-pelagic regions is  
464 predicted to start emerging in the 2040s at 500 m and 2080s at 200 m (Figure 10 k-l).

465  
466 In summary, we showed that because of the surface ocean's large warming signal and the least  
467  $pO_2$  loss outside of the polar regions under the RCP85 climate scenario, it is characterized by  
468 habitat loss in the tropics and a slight habitat gain in polar regions (Figure 11). Sea-ice melts  
469 support Oxygen gain through the enhancement of temperature-driven solubility in the surface  
470 polar regions. At depth, warming is less prevalent by the end of the 21st century; however,  
471 oxygen loss related to the weakening ventilation of the ocean interior as the ocean becomes more  
472 stratified has a stronger impact on metabolic reliance, leading to habitat loss in tropics and  
473 subtropics. On the other hand, cooler temperatures and efficient ventilation in polar regions  
474 create an oxygen-rich environment. Thus, in contrast to tropical and subtropical regions,  
475 warming leads to a slight habitat gain (Figure 11), as organisms escape the cold intolerance  
476 imposed by molecular gas diffusion at low temperatures.



477

478 **Figure 11.** Summary Figure: It shows the distribution of ecotype viability within representative ocean temperature  
 479 and  $pO_2$  boundaries for the 66 species analysed in this study. The markers represent the subsampled regions, with  
 480 polar regions denoted by circles, tropical regions by squares, and subtropical regions by stars. The colours represent  
 481 the depth levels; 50 m (grey), 200 m (purple), and 500 m (red). Each arrow shows the estimated joint temperature-  
 482  $pO_2$  climate change vector based on the net changes in temperature and  $pO_2$  (as depicted in Figure 6).

483

#### 484 **4. Discussion**

485

486 The human-induced rapid warming of the planet has been shown to drive ocean deoxygenation  
 487 (Ito et al., 2017; Schmidtko et al., 2017; Long et al., 2016). Higher metabolic oxygen demand at  
 488 higher temperatures (Gillooly et al., 2001; Deutsch et al., 2015, 2022) raises concerns about the  
 489 ability of marine ectotherms to support aerobic respiration in the future. This study set out to  
 490 characterize the anticipated climate change signal in the ocean's metabolic state in the context of  
 491 natural variability using the metabolic theory as a basis to examine the capacity of the  
 492 environment to support ectothermic marine heterotrophs.

493

494 The spatial variation in  $pO_2$  and temperature in the unperturbed natural climate state set  
495 biogeographic boundaries based on ectotherms' physiological performance. The resilience of  
496 these ectotherms' biogeographic structure to natural variability and long-term climate warming is  
497 perturbed by the joint  $pO_2$ -temperature changes, effectively measured by the metabolic index  
498 ( $\Phi'$ ). An increase in the capacity of the organisms to support aerobic respiration increases  $\Phi'$ ; for  
499 example by ocean cooling or increase in oxygen supply contrary, warming and decrease in  
500 oxygen supply decrease  $\Phi'$ . There are exceptions in extremely low-temperature environments  
501 (Figure 11), where aerobic respiration is also limited by kinematic gas transfer into the organism  
502 in addition to environmental oxygen supply. Relative changes in  $pO_2$  and temperature in the  
503 natural variability and forced trend, therefore, regulate ectotherms' resilience to environmental  
504 changes. Under the RCP85 climate scenario, the ocean generally warms homogeneously but  
505 concurrent  $pO_2$  changes are heterogeneous and vary with depth. Thus, the characteristics of these  
506  $pO_2$ -temperature forced trend changes determine when the climate change impact on marine  
507 ectotherms can be distinguishable from natural variability.

508

509 In the surface ocean,  $pO_2$  is generally abundant and relatively uniform, and thus spatial  
510 temperature variations have a dominant constraint on the spatial variations of organismic  
511 metabolic state. The warmest parts of the surface ocean, the tropical oceans, can only support  
512 about 10-20 (~ 30%) of the 61 ecotypes while cooler regions in extratropics have nearly 100%  
513 viability. Moreover, since warming anomalies propagate from the surface, the surface tropical  
514 oceans also show the largest natural variance in temperature and ecotype viability. This is  
515 because extremely warm temperatures in the surface tropics ( $>25^\circ\text{C}$ ) are mainly suited for  
516 organisms with high-temperature sensitivity ( $E_o$ ), which are relatively fewer, and mostly close to  
517 their physiological limits (Storch et al., 2014). Large natural variability in these warmest parts of  
518 the tropical surface ocean precludes the forced trend signal from emerging from the natural  
519 variability in the ecotype viability by end of the century although the ocean warms the largest in  
520 the surface. Nevertheless, the large warming trends in the surface ocean generally emerge  
521 relatively early (the 2020s) from natural variability in both temperature and ecotype viability in  
522 most regions. Minimal changes in surface  $pO_2$  in the forced trend affirm that surface ocean  
523 marine ectotherms are mainly perturbed by temperature in the context of anthropogenic changes.  
524 In polar regions, warming has a counterintuitive effect on marine ectotherms with respect to



525 most parts of the surface ocean. There, warming helps organisms escape extreme cold  
526 intolerances by enhancing membrane kinematic gas transfer which enhances  $\Phi'$  and thus ecotype  
527 richness in the future (Figure 11)

528

529 In the epipelagic and mesopelagic regions (200 m and 500 m), the forced temperature trend and  
530 natural variability are broadly smaller than the surface ocean, while  $pO_2$  changes show the  
531 opposite. Thus, at depth  $pO_2$  play a more intricate role in perturbing marine ectotherm habitats  
532 in the context of anthropogenic warming with respect to the surface ocean, where temperature  
533 plays a dominant role. Contrasting the regression between  $pO_2$  and temperature in the natural  
534 climate, and forced trends provides an instructive framework to analysing ectotherms' long-term  
535 changes. Regions showing different correlations between temperature and  $pO_2$  in the forced  
536 trends in comparison to the natural climate suggest a loss metabolic resilience; loss of habitat,  
537 and these regions tend to have a relatively early ToE. For instance, in the epipelagic and  
538 mesopelagic North Pacific, temperature- $pO_2$  regressions switched from a positive correlation in  
539 the unperturbed climate to a strong negative correlation in the forced trend (Figure 7). The North  
540 Pacific pelagic – epipelagic regions is projected to lose nearly half of the present climate ecotype  
541 viability by end of the 21<sup>st</sup> century, the projected habitat loss start emerging by the late 2030s  
542 under the RCP85 climate scenario, On the other hand, in the Arctic Ocean and some parts of the  
543 Southern Ocean, same sign  $pO_2$ -temperature correlations in the forced trends result in the  
544 preservation of the marine habitat and even slight enhancements.

545

## 546 **5. Conclusions**

547

548 The joint temperature-oxygen metabolic framework in this study provides additional insight into  
549 the impact of climate change on marine ecosystems in comparison to the independent oxygen or  
550 temperature analysis. We here showed that while warming is the leading order driving  
551 mechanism of climate change, the direct effect of warming on marine ecosystems is mostly in  
552 the upper ocean. Climate change-related oxygen loss is a major driver of marine ecosystem stress  
553 in addition to warming at depth. Incorporating organismal physiological sensitivity to oxygen-  
554 temperature changes in the metabolic framework provides insight into how climate impacts the

555 biogeographic structure of marine habitat. We find that forced perturbations to pO<sub>2</sub> and  
556 temperature will strongly exceed those associated with the natural system in many parts of the  
557 upper ocean, mostly pushing organisms in these environments closer to or beyond their  
558 physiological limits. Climate warming is expected to drive significant marine habitat loss in the  
559 surface tropical oceans and epipelagic - pelagic North Pacific Basin, while gaining marginal  
560 habitat viability in the surface Arctic Ocean and some parts of the Ocean Southern.

561

## 562 **6. Competing interests**

563 The contact author has declared that none of the authors has any competing interests

564

## 565 **7. Acknowledgments**

566

567 PM, ML, CD and TI were funded by the National Science Foundation (NSF) grant agreement  
568 No. 1737158. PM and YSF were also funded by the European Union's Horizon 2020 research  
569 and innovation programme under grant agreement No. 820989 (COMFORT). ). We also would  
570 like to acknowledge the data access and computing support provided by the NCAR Cheyenne  
571 HPC.

## 572 **8. Author contribution**

573

574 PM and ML designed the study approach. PM developed the analysis with feedback from ML,  
575 CD and TI. PM prepared the manuscript with contributions from all co-authors.

576

## 577 **9. Data access**

578

579 The CESM1 large ensemble data used in this study can be accessed in this location:

580 <https://www.cesm.ucar.edu/community-projects/lens/data-sets>

581

## 582 **10. References**

583

584 Breitburg, D., Levin, L. A., Oschlies, A., Grégoire, M., Chavez, F. P., Conley, D. J., Garçon, V.,  
585 Gilbert, D., Gutiérrez, D., Isensee, K., Jacinto, G. S., Limburg, K. E., Montes, I., Naqvi, S. W.  
586 A., Pitcher, G. C., Rabalais, N. N., Roman, M. R., Rose, K. A., Seibel, B. A., Telszewski, M.,  
587 Yasuhara, M., and Zhang, J.: Declining oxygen in the global ocean and coastal waters,  
588 <https://doi.org/10.1126/science.aam7240>, 5 January 2018.  
589

590 Deser, C., Phillips, A., Bourdette, V., and Teng, H.: Uncertainty in climate change projections:  
591 The role of internal variability, *Clim Dyn*, 38, 527–546, [https://doi.org/10.1007/s00382-010-](https://doi.org/10.1007/s00382-010-0977-x)  
592 [0977-x](https://doi.org/10.1007/s00382-010-0977-x), 2012.  
593

594 Deutsch, C., Ferrel, A., Seibel, B., Pörtner, H. O., and Huey, R. B.: Climate change tightens a  
595 metabolic constraint on marine habitats, *Science* (1979), 348, 1132–1135,  
596 <https://doi.org/10.1126/science.aaa1605>, 2015.  
597

598 Deutsch, C., Penn, J. L., and Seibel, B.: Metabolic trait diversity shapes marine biogeography,  
599 *Nature*, 585, 557–562, <https://doi.org/10.1038/s41586-020-2721-y>, 2020.  
600

601 Deutsch, C., Penn, J. L., Verberk, W. C. E. P., Inomura, K., Endress, M.-G., and Payne, J. L.:  
602 Impact of warming on aquatic body sizes explained by metabolic scaling from microbes to  
603 macrofauna, <https://doi.org/10.1073/pnas>, 2022.  
604

605 Garcia, H. E. and Gordon, L. I.: Oxygen solubility in seawater: Better fitting equations,  
606 <https://doi.org/10.4319/lo.1992.37.6.1307>, 1992.  
607

608 Garcia, H. E. , Boyer, T. P. , Locarnini, R. A. , Antonov, J. I. , Mishonov, A. V. , Baranova, O.  
609 K. , Melissa, M. Z. , Reagan, J. R. , and Johnson, D. R. ,: WORLD OCEAN ATLAS 2013  
610 Volume 3: Dissolved Oxygen, Apparent Oxygen Utilization, and Oxygen Saturation, 75,  
611 <https://doi.org/10.7289/V5XG9P2W>, 2014.  
612

613 Gillooly, J., Brown, J., West, G., Savage, V., Charnov, E., Gillooly, J. F., Brown, J. H., West, G.  
614 B., Savage, V. M., and Charnov, E. L.: Effects of size and temperature on metabolic rate  
615 Recommended Citation, 2001.  
616

617 Hawkins, E. and Sutton, R.: Time of emergence of climate signals, *Geophys Res Lett*, 39,  
618 <https://doi.org/10.1029/2011GL050087>, 2012.  
619

620 Hoegh-Guldberg, O. and Bruno, J. F.: The Impact of Climate Change on the World’s Marine  
621 Ecosystems, *New Series*, 328, 1523–1528, <https://doi.org/10.1126/science.1185779>, 2010.

622 Howard, E. M., Penn, J. L., Frenzel, H., Seibel, B. A., Bianchi, D., Renault, L., Kessouri, F.,  
623 Sutula, M. A., McWilliams, J. C., and Deutsch, C.: Climate-driven aerobic habitat loss in the  
624 California Current System, 2020.  
625

626 Hunke, E. C. and Lipscomb, W. H.: CICE: the Los Alamos Sea Ice Model Documentation and  
627 Software User's Manual Version 4.1 LA-CC-06-012, 2010.  
628

629 Hurrell, J. W., Holland, M. M., Gent, P. R., Ghan, S., Kay, J. E., Kushner, P. J., Lamarque, J. F.,  
630 Large, W. G., Lawrence, D., Lindsay, K., Lipscomb, W. H., Long, M. C., Mahowald, N., Marsh,  
631 D. R., Neale, R. B., Rasch, P., Vavrus, S., Vertenstein, M., Bader, D., Collins, W. D., Hack, J. J.,  
632 Kiehl, J., and Marshall, S.: The community earth system model: A framework for collaborative  
633 research, *Bull Am Meteorol Soc*, 94, 1339–1360, <https://doi.org/10.1175/BAMS-D-12-00121.1>,  
634 2013.  
635

636 Ito, T. and Deutsch, C.: A conceptual model for the temporal spectrum of oceanic oxygen  
637 variability, *Geophys Res Lett*, 37, <https://doi.org/10.1029/2009GL041595>, 2010.  
638

639 Ito, T., Minobe, S., Long, M. C., and Deutsch, C.: Upper ocean O<sub>2</sub> trends: 1958–2015, *Geophys*  
640 *Res Lett*, 44, 4214–4223, <https://doi.org/10.1002/2017GL073613>, 2017.  
641

642 Kay, J. E., Deser, C., Phillips, A., Mai, A., Hannay, C., Strand, G., Arblaster, J. M., Bates, S. C.,  
643 Danabasoglu, G., Edwards, J., Holland, M., Kushner, P., Lamarque, J. F., Lawrence, D.,  
644 Lindsay, K., Middleton, A., Munoz, E., Neale, R., Oleson, K., Polvani, L., and Vertenstein, M.:  
645 The community earth system model (CESM) large ensemble project : A community resource for  
646 studying climate change in the presence of internal climate variability, *Bull Am Meteorol Soc*,  
647 96, 1333–1349, <https://doi.org/10.1175/BAMS-D-13-00255.1>, 2015.  
648

649 Keeling, R. F., Körtzinger, A., and Gruber, N.: Ocean deoxygenation in a warming world, *Ann*  
650 *Rev Mar Sci*, 2, 199–229, <https://doi.org/10.1146/annurev.marine.010908.163855>, 2010.  
651 Keil, P., Mauritsen, T., Jungclaus, J., Hedemann, C., Olonscheck, D., and Ghosh, R.: Multiple  
652 drivers of the North Atlantic warming hole, *Nat Clim Chang*, 10, 667–671,  
653 <https://doi.org/10.1038/s41558-020-0819-8>, 2020.  
654

655 Lindsay, K., Bonan, G. B., Doney, S. C., Hoffman, F. M., Lawrence, D. M., Long, M. C.,  
656 Mahowald, N. M., Moore, J. K., Randerson, J. T., and Thornton, P. E.: Preindustrial-control and  
657 twentieth-century carbon cycle experiments with the Earth system model CESM1(BGC), *J Clim*,  
658 27, 8981–9005, <https://doi.org/10.1175/JCLI-D-12-00565.1>, 2014.  
659

660 Long, M. C., Deutsch, C., and Ito, T.: Finding forced trends in oceanic oxygen, *Global*  
661 *Biogeochem Cycles*, 30, 381–397, <https://doi.org/10.1002/2015GB005310>, 2016.

662  
663 Moore, J. K., Lindsay, K., Doney, S. C., Long, M. C., and Misumi, K.: Marine ecosystem  
664 dynamics and biogeochemical cycling in the community earth system model [CESM1(BGC)]:  
665 Comparison of the 1990s with the 2090s under the RCP4.5 and RCP8.5 scenarios, *J Clim*, 26,  
666 9291–9312, <https://doi.org/10.1175/JCLI-D-12-00566.1>, 2013.

667  
668 Oschlies, A., Brandt, P., Stramma, L., and Schmidtko, S.: Drivers and mechanisms of ocean  
669 deoxygenation, <https://doi.org/10.1038/s41561-018-0152-2>, 1 July 2018.

670  
671 Penn, J. L., Deutsch, C., Payne, J. L., and Sperling, E. A.: Temperature-dependent hypoxia  
672 explains biogeography and severity of end-Permian marine mass extinction, *Science* (1979), 362,  
673 <https://doi.org/10.1126/science.aat1327>, 2018.

674  
675 Piiper, J., Dejours', P., Haab, P., and Rahn, H.: CONCEPTS AND BASIC QUANTITIES IN  
676 GAS EXCHANGE PHYSIOLOGY, *Respiration Physiology*, 292–304 pp., 1971.

677 Portner, H. O.: Climate variations and the physiological basis of temperature dependent  
678 biogeography: systemic to molecular hierarchy of thermal tolerance in animals, *Comparative*  
679 *Biochemistry and Physiology Part A*, 739–761 pp., 2002.

680  
681 Pozo Buil, M. and Di Lorenzo, E.: Decadal dynamics and predictability of oxygen and  
682 subsurface tracers in the California Current System, *Geophys Res Lett*, 44, 4204–4213,  
683 <https://doi.org/10.1002/2017GL072931>, 2017.

684  
685 Rodgers, K. B., Lin, J., and Frölicher, T. L.: Emergence of multiple ocean ecosystem drivers in a  
686 large ensemble suite with an Earth system model, *Biogeosciences*, 12, 3301–3320,  
687 <https://doi.org/10.5194/bg-12-3301-2015>, 2015.

688  
689 Rosewarne, P. J., Wilson, J. M., and Svendsen, J. C.: Measuring maximum and standard  
690 metabolic rates using intermittent-flow respirometry: A student laboratory investigation of  
691 aerobic metabolic scope and environmental hypoxia in aquatic breathers, *J Fish Biol*, 88, 265–  
692 283, <https://doi.org/10.1111/jfb.12795>, 2016.

693  
694 Schlunegger, S., Rodgers, K. B., Sarmiento, J. L., Frölicher, T. L., Dunne, J. P., Ishii, M., and  
695 Slater, R.: Emergence of anthropogenic signals in the ocean carbon cycle, *Nat Clim Chang*, 9,  
696 719–725, <https://doi.org/10.1038/s41558-019-0553-2>, 2019.

697  
698 Schmidtko, S., Stramma, L., and Visbeck, M.: Decline in global oceanic oxygen content during  
699 the past five decades, *Nature*, 542, 335–339, <https://doi.org/10.1038/nature21399>, 2017.

700 Smith, R., Jones, P., Briegleb, B., Bryan, F., Danabasoglu, G., Dennis, J., Dukowicz, J., Eden,  
701 C., Fox-Kemper, B., Gent, P., Hecht, M., Jayne, S., Jochum, M., Large, W., Lindsay, K.,

702 Maltrud, M., Norton, N., Peacock, S., Vertenstein, M., and Yeager, S.: The Parallel Ocean  
703 Program (POP) Reference Manual Ocean Component of the Community Climate System Model  
704 (CCSM) and Community Earth System Model (CESM) 1, 2010.  
705

706 Storch, D., Menzel, L., Frickenhaus, S., and Pörtner, H. O.: Climate sensitivity across marine  
707 domains of life: Limits to evolutionary adaptation shape species interactions, *Glob Chang Biol*,  
708 20, 3059–3067, <https://doi.org/10.1111/gcb.12645>, 2014.  
709

710 Tiano, L., Garcia-Robledo, E., Dalsgaard, T., Devol, A. H., Ward, B. B., Ulloa, O., Canfield, D.  
711 E., and Peter Revsbech, N.: Oxygen distribution and aerobic respiration in the north and south  
712 eastern tropical Pacific oxygen minimum zones, *Deep Sea Res 1 Oceanogr Res Pap*, 94, 173–  
713 183, <https://doi.org/10.1016/j.dsr.2014.10.001>, 2014.  
714

715 Vaquer-Sunyer, R. and Duarte, C. M.: Thresholds of hypoxia for marine biodiversity, 2008.  
716  
717